

LIGHT MODULATION

PACS numbers: 42.79.Jq; 42.62.Fi; 42.25.Fx
DOI: 10.1070/QE2010v040n05ABEH014074

Compact acousto-optic modulator operating in the purely Raman – Nath diffraction regime as a phase modulator in FM spectroscopy

V.N. Baryshev, V.M. Epikhin

Abstract. **We report fabrication of a new acousto-optic modulator (AOM-RN) operating purely in the Raman – Nath diffraction regime. This device can be used as an external phase modulator in frequency-modulation (FM) optical heterodyne spectroscopy for fast and broadband frequency control of diode lasers. The AOM-RN design is significantly simplified, and its dimensions are minimised due to a decrease (by almost an order of magnitude in comparison with the existing AOMs) in the acousto-optic interaction length and the absence of impedance matching circuit. The FM spectroscopy based on AOM-RN makes it possible to analyse both absorption and dispersion properties of optical resonances under study; this possibility is shown by the example of saturated-absorption resonances in cesium vapour. The possibility of detecting coherent population trapping resonances using FM spectroscopy with AOM-RN as an external phase modulator is experimentally demonstrated.**

Keywords: *diode laser, FM sideband heterodyne spectroscopy, acousto-optic modulator, Raman – Nath diffraction, coherent population trapping (CPT) resonances.*

1. Introduction

A new method for the frequency control of external-cavity diode lasers (ECDLs), which does not require direct modulation of the injection current, was reported in [1]. The frequency-modulation (FM) sideband heterodyne technique, in which an acousto-optic modulator (AOM) operating in the Raman–Nath diffraction regime is used as an external phase modulator, was applied to obtain error signals for frequency tuning of the diode laser to the saturated-absorption resonances of the D_2 line of cesium atoms. Currently, FM spectroscopy [2 – 4] with an electro-optic modulator (EOM) playing the role of external phase modulator is widely used to obtain error signals for high-speed electronic feedback servo-loops.

V.N. Baryshev, V.M. Epikhin State Scientific Center 'All-Russia Research Institute of Physicotechnical and Radio Measurements', 141570 Mendeleevo, Moscow region, Russia; e-mail: baryshev@aspnet.ru, epikvm@mail.ru

Received 10 February 2009; revision received 15 March 2010
Kvantovaya Elektronika **40** (5) 431 – 436 (2010)
Translated by Yu.P. Sin'kov

According to [1], the application of AOM as an external phase modulator in FM spectroscopy has some advantages over the use of EOM as a phase modulator. The main advantage is the possibility of obtaining an error signal with a desired slope sign of its linear central part in a wide frequency range, which is easily achieved by varying the frequency of the amplified local oscillator signal without changing its power. The local oscillator signal power that is necessary to ensure a few-percent ratio of powers of each $\pm$1st diffraction order sidebands to the carrier power did not exceed 100 mW. Actually, the existing EOMs do not produce a pure FM spectrum. Hence, one has to control the polarisation of the input and output beams to remove the residual amplitude noise. When using AOM, such control is not required and the experimental setup is simplified.

In this paper, we present an acousto-optic modulator of a new type with a 2-mm acousto-optic interaction length: AOM-RN. This device, designed to operate in the purely Raman – Nath diffraction regime, was applied as an external phase modulator in the FM sideband heterodyne technique for frequency control of the ECDL. The character of the dependence of the beat-signal-induced photocurrent and error signal amplitude on the acousto-optic interaction length suggested that the AOM-RN design can be considerably simplified and the modulator dimensions can be minimised, mainly by shortening the acousto-optic interaction length by almost an order of magnitude in comparison with the existing AOMs.

Error signals corresponding to narrow coherent population trapping (CPT) resonances were obtained using FM spectroscopy with an AOM-RN as an external phase modulator.

2. Theoretical background

The application of AOM in the Raman – Nath diffraction regime as a phase modulator in FM optical heterodyne spectroscopy [2, 3] appears to be reasonable, because in the case of weak AOM excitation, due to the phase modulation, its modulator output spectrum may consist of a strong carrier and two weak sidebands corresponding to the $\pm$1st diffraction orders.

The Raman – Nath diffraction regime was described in detail in the literature (see, for example, [5]). A sinusoidal acoustic wave with a length Λ and frequency Ω, propagating in a single crystal at a speed v_s, induces periodic variations in the refactive index n compared to its initial mean value n_0.

The electric field E_1 of a light wave incident on a single crystal orthogonally to the axis of an acoustic beam of width L (the acousto-optic interaction length), after the passage through the AOM, is described by the expression

$$E_1(t) = \frac{E_0}{2} \sum_{N=-\infty}^{\infty} J_N(\Delta\Phi) \exp[\mathrm{i}(\omega + \Omega)\tau] + \psi.\psi., \qquad (1)$$

where the modulation index $\Delta\Phi$ is equal to the wave phase modulation amplitude $(2\pi L/\lambda_0)\Delta n$, induced by the variable part Δn of the refractive index; λ_0 is the light wavelength in vacuum; and ω is the carrier frequency. The amplitude dependence of the carrier and sidebands on the phase shift $\Delta\Phi$ is given by the Bessel functions $J_N(\Delta\Phi)$.

The amplitude of variation in the refractive index Δn is proportional to the square root of the sound wave intensity $I_s = P_s/(LH)$, where H is the width of the acousto-optic interaction region (or the light beam diameter) and P_s is the sound power. Thus, the phase modulation amplitude of the light wave is proportional to the square root of the acousto-optic interaction length:

$$\Delta\Phi = (2\pi L/\lambda_0)\Delta n \sim L^{1/2}. \qquad (2)$$

For example, for the TeO_2 crystal [6] (with $n = 2.367$, $v_s = 4.2$ km s^{-1}, density $\rho = 6.0 \times 10^3$ kg m^{-3}, and photoelastic constant $p = 0.24$), at $\lambda_0 = 850$ nm, $P_s = 40$ mW, and the width of acousto-optic interaction region $H = 2$ mm, according to [7], $\Delta\Phi = (2\pi L/\lambda_0)\Delta n = (2\pi L/\lambda_0)(n_0^3 p/2)\times (2I_s/\rho v_s^3)^{1/2} = 0.47$ rad at $L = 15$ mm and $\Delta\Phi = 0.16$ rad at $L = 2$ mm.

The latter example ($\Delta\Phi = 0.16$ rad at $L = 2$ mm) corresponds to the parameters chosen below for the AOM-RN designed for operation in the purely Raman–Nath diffraction regime. Therefore, it would be logical to assume that $\Delta\Phi \ll 1$, $J_0(\Delta\Phi) \simeq 1$, $J_{\pm1}(\Delta\Phi) = \pm\Delta\Phi/2$, and the higher order sidebands are negligible. Thus, the spectrum of the light transmitted through the AOM operating in the Raman–Nath diffraction regime, contains a strong carrier at a frequency ω and two weak sidebands at $\omega \pm \Omega$ and with amplitudes $|E_0(\Delta\Phi/2)|$, diverging at an angle $\vartheta_1 = \pm(\lambda/\Lambda)$ symmetrically relative to the incident direction of the input light.

Then, the optical beam passes through a dispersive medium of length l, whoseintensity-absorption coefficient α and the refractive index n are functions of optical frequency. Taking into account the amplitude attenuation $\delta_N = \alpha_N l/2$ and the optical phase shift $\phi_N = n_N l(\omega + N\Omega)/c$ (where $N = -1, 0, 1$ denotes the values of the frequencies $\omega - \Omega$, ω, $\omega + \Omega$, respectively) experienced by each frequency component, we arrive to the following expression (similar to that derived in [2, 3]) for the light intensity $I_2(t) = c|E_2(t)|^2/8\pi$ incident on a photodetector:

$$I_2(t) = \frac{c|E_2|^2}{8\pi} = \frac{cE_0^2}{8\pi} \mathrm{e}^{-2\delta_0}[1 + (\delta_{-1} - \delta_1)$$

$$\times \Delta\Phi \cos\Omega t + (\phi_1 + \phi_{-1} - 2\phi_0)\Delta\Phi \sin\Omega t], \qquad (3)$$

where the $\cos\Omega t$ component of the beat signal is proportional to the difference in loss experienced by the upper and lower sidebands, whereas the $\sin\Omega t$ component is proportional to the difference between the phase shift of the carrier and the average phase shifts of the sidebands. The null beat signal is the result of the phase modulation of light and perfect compensation for the rf signal arising from the upper sideband beating against the carrier by the rf signal from the lower sideband beating against the carrier.

The beat-signal-induced photocurrent of the photodetector is proportional to the modulation index $\Delta\Phi$. Hence, as follows from (2), it is proportional to $L^{1/2}$. The decrease in the acousto-optic interaction length by an order of magnitude reduces the beat signal by a factor of 3. In principle, it can be compensated for by an increase in the optical power, because beats are proportional to the geometric mean of the carrier intensity and the intensity of some sideband, i.e., to $E_0^2\Delta\Phi$.

In our experiment the dispersed medium of length l through which FM light was transmitted was a cell with saturated cesium vapour. The sampled transitions are the saturated absorption resonances of the Cs D_2 line in the field of counterpropagating waves, one of which (saturating absorption) has a carrier frequency ω, and the probe field is formed by the output AOM radiation. The latter consists of three beams, which correspond to the carrier and the nearest sidebands of the $\pm$1st diffraction order, with the frequencies $\omega \pm \Omega$. The resonant absorption at the frequency ω_0 takes place when the saturating beam interacts with the atoms that are in resonance with the field of any of the sidebands. The case when the atoms with a nonzero velocity projection on the saturating beam direction (V_z) are in resonance with the probe field of the upper sideband is shown in Fig. 1. For this group of atoms the resonant frequency (with allowance for the Doppler detuning) is

$$\omega_0 = (\omega + \Omega)(1 - V_z/c), \qquad (4)$$

where c is the speed of light. For the same group of atoms, upon resonant interaction with the counterpropagating saturating carrier field, the resonant frequency has the form

$$\omega_0 = \omega(1 + V_z/c). \qquad (5)$$

Taking into account the condition $\Omega \ll \omega$, we find from (4) and (5) that $\omega = \omega_0 - \Omega/2$. When the probe radiation is formed by the lower frequency sideband, the carrier frequency is $\omega = \omega_0 + \Omega/2$. Thus, according to (3), the

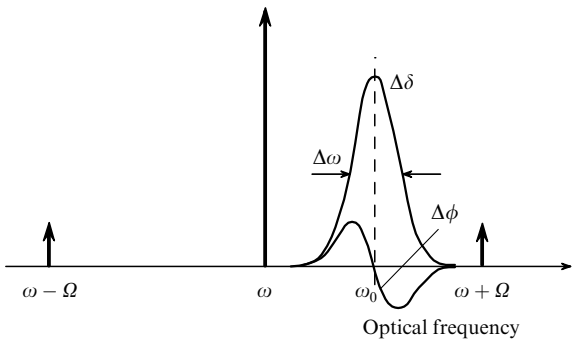

Figure 1. Spectrum of light transmitted through AOM-RN, and an illustration of FM spectroscopy in the saturated-absorption configuration when the resonant line with a frequency ω_0 and width $\Delta\omega$ is probed by the upper sideband.

absorption-related beat signal, and, therefore, the corresponding error signal, should contain two resonances with amplitudes of opposite sign, frequency-spaced by $2\Omega/2$.

3. Experimental setup

A schematic of the experimental setup was shown in Fig. 1 in [1]. ECDLs provided tunable monochromatic 851-nm radiation. The modulator was ISOMET 1205-C2 AOM with a central operating frequency of 80 MHz and a sweep bandwidth of 40 MHz, driven by 40 mW of the rf power at frequencies (in the range from 10 to 40 MHz) large compared to the 5 MHz of the natural linewidth of the optical transitions in the Cs D_2 line.

1205-C2 AOM was designed for operating in the Bragg deviation regime, at frequencies much higher than the ones we obtained error signals for. The AOM diffraction properties and characteristics in the desired frequency range (10–40 MHz) are intermediate between those corresponding to the two limiting cases of purely Raman–Natt diffraction or purely Bragg deflection regimes. According to [8], the limiting conditions are determined by the dimensionless Klein–Cook factor $Q = 2\pi L\lambda/\Lambda^2$, where L is the acousto-optic interaction length; λ and Λ are the light and acoustic wavelengths, respectively. The range $Q < 0.3$ corresponds to the Raman–Nath diffraction, while the Bragg diffraction regime is dominant at $Q > 4\pi$. The estimates for the 1205-C2 AOM give $Q = 3.1$ for $\Omega = 40$ MHz and $Q = 0.75$ for $\Omega = 20$ MHz.

If AOM operates in the mixed diffraction regime and does not produce a pure FM spectrum, as it should occur due to the phase modulation in the Raman–Nath diffraction regime at normal incidence of the input optical beam, small imbalance in the amplitudes of the sidebands or their relative phase shift can prevent the total beat signal at the photodetector from vanishing exactly and can introduce nonzero baseline of the error signals and additional amplitude noise.

To avoid these problems and obtain a frequency-modulated spectrum at the AOM output, we developed and designed AOM-RN for operation purely in the Raman-Nath diffraction regime. This modulator has a center working frequency of 30 MHz and a modulation bandwidth of 20 MHz. Its acousto-optic interaction length is 2 mm.

For this new modulator, the parameter Q is 0.41 and 0.1 at modulation frequencies of 40 and 20 MHz, respectively. At such Q values, Raman–Nath diffraction regime is dominant, and Bragg deflection of the light mainly into one beam of the first diffraction order is not observed yet, even when the incidence angle is comparable with the Bragg incidence angle. At the same 40 mW of the driving AOM-RN rf power, the zero background level of the error signals was achievable for all of the sub-Doppler resonances without noticeable losses in the amplitude of the signals compared with those obtained when 1205-C2 AOM was used.

The acousto-optic duct in AOM-RN is a TeO_2 single-crystal prism, approximately $5 \times 5 \times 5$ mm in size. A $LiNbO_3$ single-crystal plate, glued to the acoustic plane of the duct, was used as a piezoelectric transducer of longitudinal ultrasonic wave (USW). The plate thickness corresponds to a resonant frequency of 30 MHz. The impedance matching circuit is the impedance transformer for the piezoelectric transducer and rf channel (50 Ω); it ensures AOM-RN operation in a frequency band of 20–40 MHz.

The value of the driving AOM-RN rf power that is necessary to ensure sufficient (for FM spectroscopy) power ratios of the sidebands and the carrier, $P_{\pm1}/P_0$, turned out to be small (40 mW); therefore, we tried to do without the electronic matching circuit. The same rf power (40 mW) was applied directly to the piezoelectric transducer through an RF cable. The standing wave ratio (SWR) at a modulation frequency of 40 MHz was measured for one of the experimental samples. These measurements showed that the rf power transferred to the piezoelectric transducer (P_s) is lower than the supplied rf power by a factor of 2. Since $\Delta\Phi_s \sim P_s^{1/2}$, a twofold decrease in the rf power leads to a decrease in the error signal amplitude by approximately 30 %; however, the rejection of the matching circuit allows one to reduce the AOM-RN dimensions even more. Figure 2 shows a photograph of 1205-C2 AOM and two AOM-RN samples with an acousto-optic interaction length of 2 mm. Thus, the decrease in the acousto-optic interaction length and rejection of the impedance matching circuit made it possible to decrease in size the acousto-optic crystal and, correspondingly, to minimise the dimensions of the modulator designed for operation purely in the Raman–Nath diffraction regime and providing the zero background level of error signals.

Figure 2. Photograph of 1205-C2 AOM and two AOM-RN samples.

4. Results and discussion

In the experimental configuration typical of the saturated absorption spectroscopy, whose mechanism is clarified in Fig. 1, we investigated how the profile of the error signals (Figs 3, 4) produced by AOM-RN agrees with the theory of FM spectroscopy [2–4]. According to [3], if the modulation frequency Ω is smaller than the spectral linewidth, the amplitude of the $\cos\Omega t$ component of the beat signal is proportional to the derivative of the absorption coefficient, whereas the amplitude of the $\sin\Omega t$ component is proportional to the second derivative of dispersion. At the same time, the error signals, corresponding to either absorption or dispersion, can be obtained directly if the phase relation for the mixer input signals is properly chosen. In the case under consideration such a relation can be implemented by varying the frequency of the local oscillator, if the modulation frequency Ω is sufficiently high or the

resonance is sufficiently narrow to ensure sampling of the optical resonance under study by an only isolated sideband, as shown in Fig. 1. Thus, the error signal profile depends strongly on the $2\Omega/\Delta\omega$ ratio (the ratio of the frequency range between the sidebands, generated by AOM-RN, and the width of the saturated-absorption and CPT resonances under study). We varied the intensities of the saturating and probe fields, thus changing the $2\Omega/\Delta\omega$ ratio at a fixed modulation frequency Ω. The saturating field intensity was always lower than that of the probe field by a factor of 2. The carrier frequency was scanned near an isolated saturated-absorption resonance at two different probe field intensities. When recording curves (*1*) in Figs 3 and 4, the saturation parameters for the probe and saturating fields exceeded the corresponding values for curves (*2*) by a factor of 4.

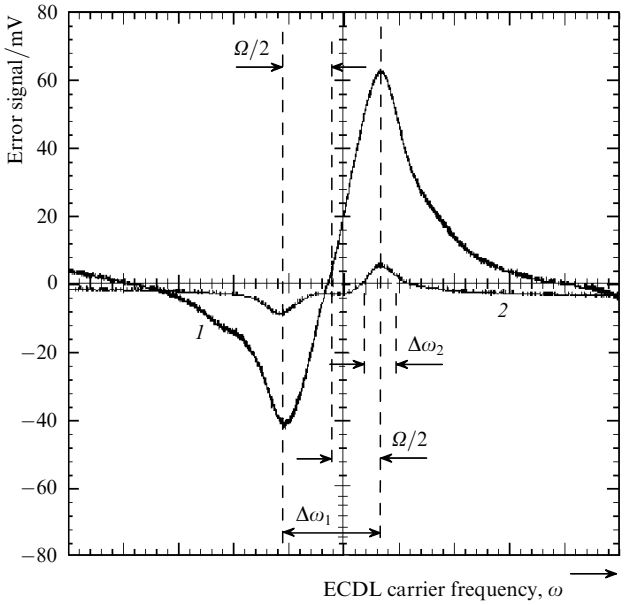

Figure 3. Error signals with a dominant absorption component for $\Omega = 25.76$ MHz and two values of laser power at the AOM-RN input: (*1*) 7 and (*2*) 1.75 mW.

Curves (*2*) in Figs 3 and 4 are the experimental error signals with dominance of the components corresponding to absorption or dispersion [see expression (3)]. The signal corresponding to the absorption clearly shows a negative-going signal with a width $\Delta\omega_2$, which reproduces the absorption line shape probed by the upper sideband, followed at a spacing $2(\Omega/2)$ by a positive-going signal, which reproduces the same absorption line shape probed by the lower FM sideband. For signal (*2*) the ratio $2\Omega/\Delta\omega_2 \approx 6$. As can be seen in Fig. 3, when the saturation parameter increases by a factor of 4, the resonance FWHM $\Delta\omega_1$ is equal to the difference in the frequencies of the extrema of error signal (*1*) (whose profile corresponds to the derivative of absorption), i.e., to the modulation frequency: $\Delta\omega_1 = 2(\Omega/2) = \Omega$. In this case, $2\Omega/\Delta\omega_1 = 2$. The shape of the experimentally obtained error signals corresponding to absorption qualitatively coincides with that theoretically calculated in [3] for approximately the same $2\Omega/\Delta\omega$ values.

The signal corresponding to dispersion at a small saturation parameter [Fig. 4, curve (*2*)], shows three over-

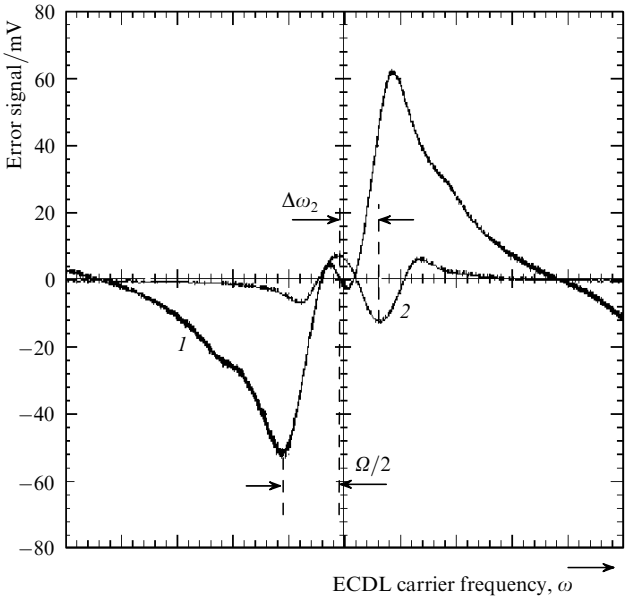

Figure 4. Error signals with a dominant dispersion component for $\Omega = 26.02$ MHz and two values of laser power at the AOM-RN input: (*1*) 7 and (*2*) 1.75 mW. Curves (*1*) and (*2*) are slightly shifted with respect to each other along the abscissa axis (without changing the scale) to make them more illustrative.

lapping dispersion-like curves, which occur due to the successive resonant interaction of all three components of the probe field.

Then we investigated the potential of FM spectroscopy for detecting narrow CPT resonances [9] or dark resonances in saturated cesium vapour. Figure 5 shows a schematic of the experimental setup for detecting the error signals corresponding to CPT resonances in a magnetically unshielded cell with saturated cesium vapour (without buffer gas) at room temperature.

Two light waves from two independent lasers, ECDL1 and ECDL2, propagating in the same direction, equally linearly polarised, and matched in space, couple both hyperfine sublevels of the ground state with the common excited hyperfine sublevel (Fig. 6). The ECDL2 carrier

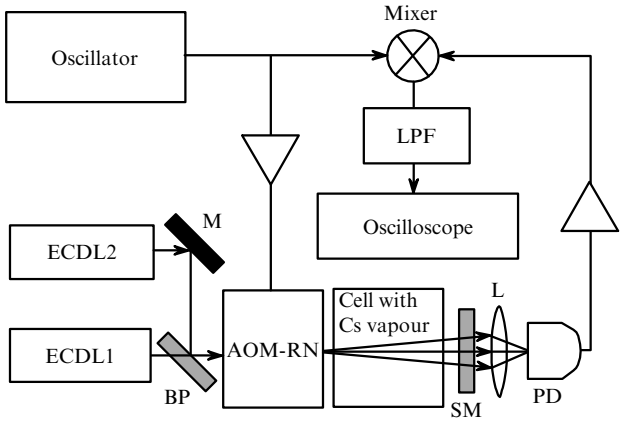

Figure 5. Schematic of the experimental setup for detecting CPT resonances: (ECDL) external-cavity diode laser, (BS) beamsplitter, (L) lens, (PD) photodetector, (LPF) low-pass filter, (M) mirror, and (SM) semitransparent mirror.

frequency is fixed near the $6S_{1/2}$, $F = 3 \leftrightarrow 6P_{3/2}$, $F' = 4$ transition, while the ECDL1 carrier frequency is scanned over the Doppler line corresponding to the $6S_{1/2}$, $F = 4 \leftrightarrow 6P_{3/2}$, $F' = 3, 4, 5$ transitions. The frequency scan is performed by applying a saw-tooth voltage to the piezoceramic converter, which controls the external cavity length. Curve (*1*) in Fig. 7 is the error signal corresponding to saturated absorption, when a semitransparent mirror forms counterpropagating saturating radiation. At this instant the ECDL2 radiation is blocked at the AOM-RN input and does not arrive at the photodetector. Curve (*2*) in Figs 7 and 8 is the same error signal but in the absence of saturating radiation, when the semitransparent mirror is removed from the optical scheme. In this case, the experimental configuration of FM spectroscopy corresponds to that described in [2, 3]. When the ECDL2 radiation with a fixed frequency is unblocked, the frequency-modulated radiation from both lasers enters the cell and arrives at the photodetector; as a result, the oscillogram [selected portion A on curve (*3*) in Fig. 8] contains three pronounced successive dispersion signals, which are separated by a frequency range Ω and correspond to CPT resonances. The latter are formed upon successive scanning the frequency ω_{dl1} by the higher frequency sideband, carrier, and lower frequency sideband at the instants when the differences between their frequencies and the fixed ECDL2 carrier frequency coincide with the frequency splitting between two hyperfine sublevels of the Cs ground state. Each of these three signals is the result of superposition of the error signals corresponding to all possible two-photon CPT resonances in the three-level systems formed by split and shifted magnetic sublevels in the Λ configuration [10]. To estimate the width of the CPT resonances in Fig. 9, we present portion A of curve (*3*) in Fig. 8 on an enlarged scale. One can see that the width of all three resonances does not exceed the natural width of the excited level (5 MHz). The linewidth of the CPT resonances and the corresponding error signals in our experiment is determined by a number of effects and parameters such as power broadening, transit-time-induced broadening, splitting and shift of the magnetic sublevels in an external magnetic field, and, in the case of two independent, free-running lasers, mainly by the total spectral width of their radiation, which we estimated to be 2 MHz. For a magnetically unshielded cell in the Earth's magnetic field with an induction $B \approx 0.5\times\ 10^{-4}$ T, the maximum frequency shift [10] of possible Λ resonances with respect to the unperturbed Λ resonance, which couples the magnetic sublevels of the ground state, $m_3 = 0$ and $m_4 = 0$, for the cesium atom is $\pm\Delta\omega = \pm(m_3 + m_4) \times (3.5\ \text{kHz}\ \mu\text{T}^{-1}) \times \text{B} = \pm(3 + 3) \times (3.5\ \text{kHz}\ \mu\text{T}^{-1}) \times (0.5 \times 10^{-4}\ \text{T}) = \pm 6 \times (3.5\ \text{kHz}\ \mu\text{T}^{-1}) \times (0.5 \times 10^{-4}\ \text{T}) \approx \pm 1$ MHz. These estimates qualitatively explain the observed spectral width of the error signal, which is approximately 4 MHz.

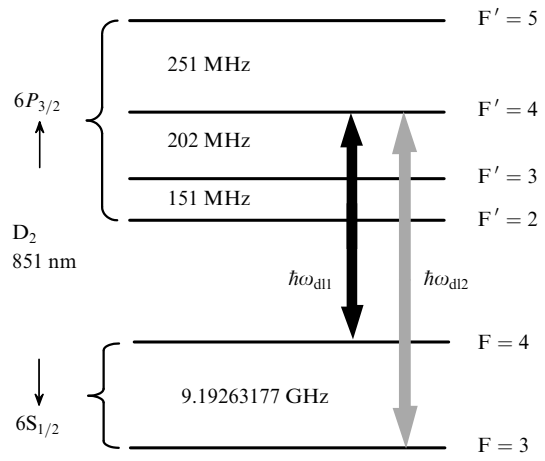

Figure 6. Energy level diagram of the Cs D_2 line.

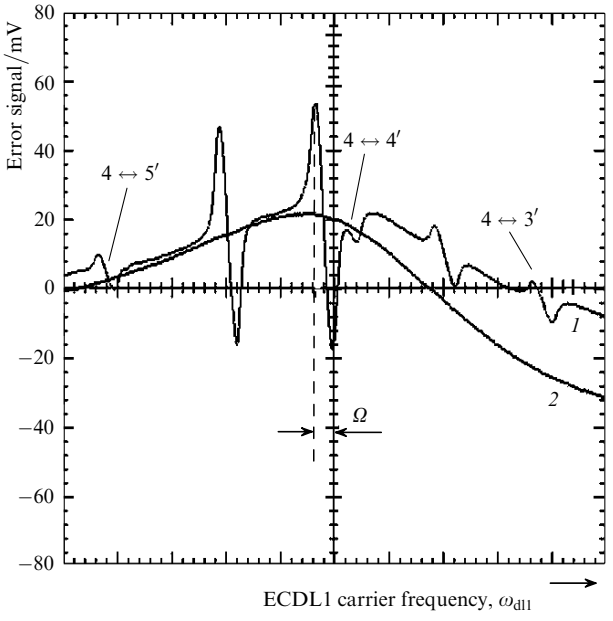

Figure 7. (*1*) Oscillogram of the error signal, which corresponds to saturated absorption, when the semitransparent mirror forms counterpropagating saturating radiation (the ECDL2 radiation is blocked at this instant). (*2*) The same error signal but in the absence of saturating radiation (without SM); $\Omega = 26.1$ MHz.

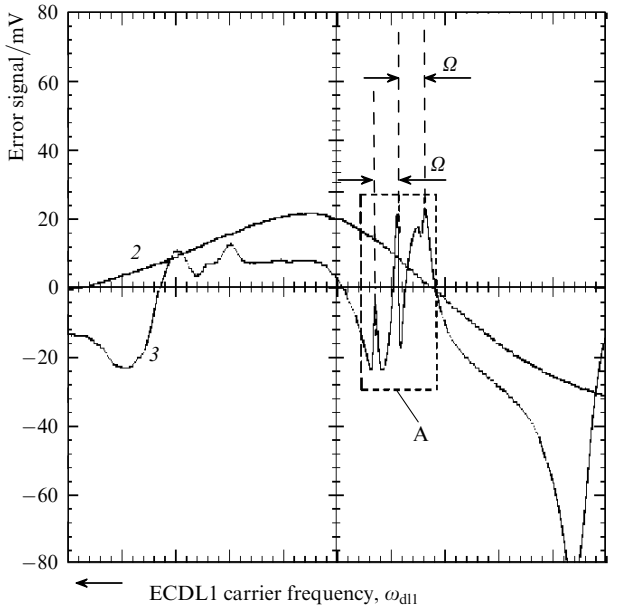

Figure 8. (*2*) The same error signal (*2*) as in Fig. 7. (*3*) The error signal after unblocking the frequency-fixed ECDL2 radiation. The recording sequence for the curves in Figs 7 and 8 is set by their serial number. The axis scales are identical in both figures; $\Omega = 26.1$ MHz.

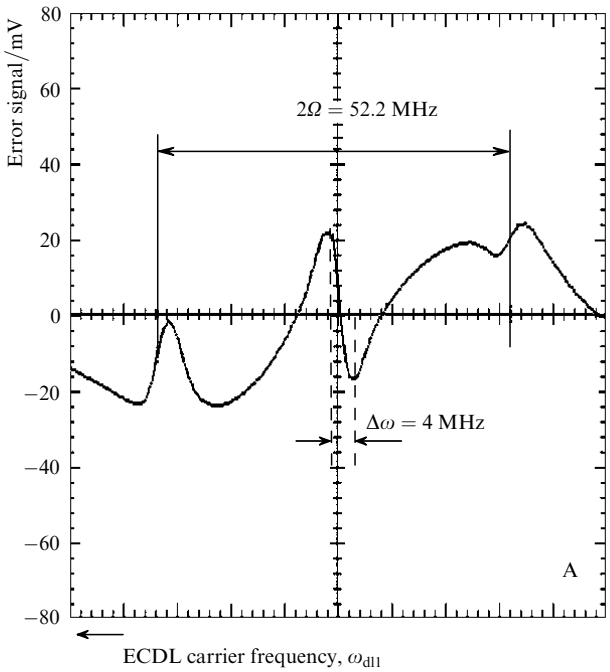

Figure 9. Portion A of curve (*3*) in Fig. 8 on an enlarged scale; $\Omega = 26.1$ MHz.

5. Conclusions

We have developed a new acousto-optic modulator, AOM-RN, with a 2-mm acousto-optic interaction length. This modulator operates purely in the Raman–Nath diffraction regime and is used as an external phase modulator FM sideband heterodyne spectroscopy for frequency tuning of ECDLs to the optical resonances. It is shown that when this diffraction regime dominates over the Bragg diffraction, the modulator design can be significantly simplified, and its dimensions can be minimised; hence, this modulator is promising for compact laser systems.

It has been shown that FM sideband spectroscopy with AOM-RN as an external phase modulator is capable of detecting both the absorption and dispersion features of the investigated optical resonances.

We have experimentally demonstrated that the detection of CPT resonances by means of FM spectroscopy with AOM-RN as an external phase modulator is possible. The zero-background error signals corresponding to these resonances can be used in feedback loops in compact atomic frequency standards based on CPT effect. The main source of frequency instability in such devices is the ac Stark shift due to the presence of non-resonant components and related frequency noise in the emission spectrum of diode lasers [11]. Therefore, the capacity of extremely high-speed laser frequency tuning provided by FM sideband heterodyne technique promises a further improvement of short-term stability of quantum frequency standards utilising CPT clock transitions.

References

1. Baryshev V.N., Domnin Yu.S., Kopylov L.N. *Kvantovaya Elektron.*, **37** (11), 1006 (2007) [*Quantum Electron.*, **37** (11), 1006 (2007)].
2. Bjorklund G. *Opt. Lett.*, **5**, 15 (1980).
3. Bjorklund G., Levenson M., Lenth W., Ortiz C. *Appl. Phys. B*, **32**, 145 (1983).
4. Hall J.L., Hollberg L., Baer T., Robinson H.G. *Laser Spectroscopy V* (Berlin–Heidelberg–New York: Springer, 1981) p. 15.
5. Born M., Wolf E. *Principles of Optics: Electromagnetic Theory of Propagation, Interference, and Diffraction of Light* (Oxford: Pergamon, 1964; Moscow: Nauka, 1970); Dieulesaint E., Royer D. *Elastic Waves in Solids* (New York: Wiley, 1976; Moscow: Nauka, 1982).
6. Blistanov A.A. et al. *Akusticheskie kristally* (Acoustic Crystals) (Moscow: Nauka, 1982).
7. Haus H.A. *Waves and Fields in Optoelectronics* (Englewood Cliffs: Prentice-Hall, 1984; Moscow: Mir, 1988).
8. Uchida N., Niizeki N. *Proc. IEEE,* **61**, 1073 (1973).
9. Alzetta G., Gozzini A., Moi L., Orriols G. *Nuovo Cimento B*, **36**, 5 (1976).
10. Wynands R., Nagel A., Brandt S., Meschede D., Weis A. *Phys. Rev. A*, **58**, 196 (1998).
11. Kargapol'tsev S.V., Velichanskii V.L., Vasil'ev V.V., Kobyakova M.Sh., Morozyuk A.V., Shiryaeva N.V., Konyaev V.P. *Kvantovaya Elektron.*, **39** (6), 487 (2009) [*Quantum Electron.*, **39** (6), 487 (2009)].